16TH EUROPEAN CONFERENCE ON EARTHQUAKE ENGINEERING THESSALONIKI 18 - 21 JUNE 2018

# A PROBABILISTIC FRAMEWORK FOR ASSESSING LIQUEFACTION DAMAGE IN URBAN AREAS: APPLICATION TO CHRISTCHURCH (NZ)

Nikolaos NTRITSOS[1] and Misko CUBRINOVSKI[2]

## ABSTRACT

This paper presents a probabilistic procedure for mapping liquefaction damage in urban areas using Monte Carlo simulations and advanced effective stress analyses. The procedure is illustrated through its application to assess the liquefaction damage in two sub-regions of Christchurch, New Zealand under the shaking induced by the 22 February 2011 Christchurch earthquake. The two sub-regions have vastly different subsurface profile characteristics which are reflected in their vastly different performance during the 2010–2011 Canterbury earthquakes. Selected sites from the two sub-regions are used for the design and calibration of a probabilistic model for the randomization of soil profiles. The probabilistic model consists of two main components: a model that describes the random stratigraphy at each sub-region (i.e. the location of layer boundaries and thicknesses of layers) and a model that describes the soil properties including their variation within each layer. The uncertainty in the ground motion is also considered in the analysis by utilizing both recorded and (physics-based) simulated motions together with a random scaling factor. The probabilistic analysis yields results that are in very good agreement with the actual observations of liquefaction damage from the 22 February 2011 Christchurch earthquake, and explains the vastly different performances of no-liquefaction manifestation and severe liquefaction cases, which could not be explained by the simplified procedures. However, important mechanisms of the system response cannot be easily detected in such analyses and hence, detailed deterministic effective stress analyses are necessary for identification of key mechanisms and correct interpretation of the results.

*Keywords: Earthquake damage; Effective stress analysis; Liquefaction; Probabilistic; Uncertainty*

## 1. INTRODUCTION

Liquefaction assessments (i.e. evaluation of liquefaction triggering potential and consequences) are routinely carried out by geotechnical engineers using deterministic empirical methods which are largely based on observations from case histories (e.g. Boulanger and Idriss, 2014; Idriss and Boulanger, 2008; Robertson and Wride, 1998; Youd et al. 2001). These methods consider each layer in isolation (i.e. separately from any other layer in the deposit), and a factor of safety against liquefaction triggering, maximum shear and volumetric strains are estimated separately for each layer. In other words, interactions between different layers in the dynamic response or pore-water pressure re-distribution and water flow are ignored in these methods. Recently, Cubrinovski et al. (2017) illustrated that such system response effects can significantly influence the severity of liquefaction manifestation (and subsequent damage) at the ground surface. It is therefore important to consider alternative (more advanced) methods of analysis which are able to simulate accurately the complex dynamic response of stratified deposits as well as the development and redistribution of excess pore water pressures throughout the deposit. In this regard, fully coupled seismic effective stress analysis can provide important insights (Cubrinovski et al. 2017). However, one should not set aside the fact that even when such advanced analysis tools are implemented, the results remain specific to the particular site being modelled as well as the particular characteristics of the ground motion used as a base excitation.

In fact, liquefaction hazard analysis is strongly influenced by the uncertainties associated with the ground motion hazard, the site characterization, and the liquefaction evaluation (triggering, consequences) models.

[1]PhD Student, University of Canterbury, Christchurch, New Zealand, nikolaos.ntritsos@pg.canterbury.ac.nz
[2]Professor, University of Canterbury, Christchurch, New Zealand, misko.cubrinovski@canterbury.ac.nz

Given that implementation of state-of-the-art methods for liquefaction analysis would reduce the uncertainty associated with the liquefaction evaluation models, it remains to deal with the other two components involved, that is the variation in input ground motion and subsurface profile. Quantifying these uncertainties is of paramount importance when assessing the liquefaction vulnerability of urban areas where, on the one hand, geotechnical investigation data from only a limited number of sites are available to characterize a given area and, on the other hand, the ground motions to which these areas will be subjected in future earthquakes are substantially different in characteristics and highly variable in details. Thus, a probabilistic representation of these two components is necessary for the development of a rigorous methodology for liquefaction risk assessment of urban areas.

This paper describes a new framework for probabilistic liquefaction evaluation of urban areas based on seismic effective stress analyses. The proposed methodology uses Monte Carlo simulations to estimate the statistics of the system response due to variations in the input ground motion and soil profile. More specifically, the variation in characteristic measures of the ground response (liquefaction performance), is evaluated by analyzing different representations of the subsurface profile under an appropriate set of ground motions representing the shaking intensity of interest. The framework is illustrated through its application to assess the liquefaction performance (severity of surface liquefaction manifestation) of two sub-regions of Christchurch, New Zealand during the 22 February 2011 Christchurch earthquake.

In the following sections, key differences in the deposit characteristics and liquefaction performances of the two Christchurch sub-regions are first discussed, followed by a detailed description of the employed probabilistic soil model and the treatment of uncertainty in the input ground motion. Results from the effective stress analyses are then presented and assessed in comparison with the actual observations of liquefaction damage from the 22 February 2011 earthquake.

## 2. CONSIDERED CHRISTCHURCH SUBREGIONS

The city of Christchurch is primarily situated upon a low relief, alluvial landscape on the east coast of New Zealand's South Island. The central and eastern suburbs are predominantly underlain by alluvial sands, silts and drained peat swamps deposited during over-bank flows of the Waimakariri River (Springston formation) which are interlayered with beach, estuarine, lagoonal, dune, and coastal swamp deposits comprising gravel, sand, silt, clay, shell and peat (Christchurch formation; Brown and Weeber, 1992). Fluvial sands, silts, gravels and peats of the Springston formation are present to the west of the central city (Brown and Weeber, 1992).

In the period between September 2010 and December 2011, Christchurch was hit by a series of strong earthquakes known as the Canterbury Earthquake Sequence (CES). The earthquakes had significant geotechnical features including widespread and repeated liquefaction affecting nearly 60,000 residential buildings and properties. Particularly severe liquefaction with large volumes of soil ejecta covering nearly half of the city area occurred in the 22 February 2011 earthquake which was the most devastating earthquake in the sequence resulting in 185 fatalities. The extent of liquefaction–induced land damage caused by the 22 February 2011 earthquake is depicted in Figure 1 (NZGD, 2013). Liquefaction affected significantly the eastern suburbs of the city along the Avon River where lateral spreading also occurred (Cubrinovski and Robinson, 2016).

In this section, key differences in the deposit characteristics and liquefaction responses of two sub-regions of Christchurch that showed vastly different performance during the 2010–2011 Canterbury earthquakes are explored. The Papanui suburb is located northwest of the CBD (Central Business District) and exhibits elevations of 10–12 m asl. It got by the 2010–2011 CES with only minor liquefaction manifestation (minor quantities of ejected material and traces of liquefaction) encountered over limited areas. The Avondale suburb is located along the present day path of the Avon River and, as shown in Figure 1, and exhibits elevations of 1–3 m asl. It corresponds to some of the most widespread observations of severe liquefaction and lateral spreading related damage following the February 2011 earthquake. The two considered sub-regions are indicated with the black ovals in the map of Figure 1.

### *2.1 Papanui subsurface profile*

The subsurface profile in Papanui is largely comprised of alluvial sandy silts, clayey silts and peats of the so-called Springston formation in the upper 10 m depth, overlying primarily sands of the Christchurch formation up to the upper boundary of the Riccarton Gravel (i.e. a firm and dense gravelly material of shear wave velocity $V_s \approx 400$ m/s lying below the shallow surface deposits of Christchurch), at a depth of about 20 m from the ground surface. The shallow soil profile of a typical site in Papanui is shown in Figure 2a, in terms of soil behavior type index $I_c$ and equivalent clean sand cone tip resistance $q_{c1Ncs}$, calculated from the original Cone Penetration Test (CPT) traces using the Boulanger and Idriss (2014) liquefaction triggering procedure. The soil profile has multiple liquefiable layers of low tip resistance ($q_{c1Ncs} \approx 77$–$84$) within the top 9 m with soil behavior type index $I_c$ that varies from 1.9 to 2.3, which is consistent with soil behavior type associated with silty sands to non-plastic silts. The shallowest of these layers, at depth 1.5 m from the ground surface, which encompasses two sublayers with $q_{c1Ncs}$ = 81–83 and $I_c$ = 2.0–2.3 is identified as the critical layer for liquefaction manifestation at the ground surface (i.e. the layer that is most likely to trigger and manifest liquefaction at the ground surface). All liquefiable layers up to 8 m depth are relatively thin, with 1.0 m maximum thickness and are sandwiched between non-liquefiable soils of $I_c > 3.0$. In particular, the shallow critical layer is overlying a non-liquefiable clayey layer of 2.5 m thickness and is overlaid by a 1.5 non-liquefiable crust. This vertical discontinuity of low resistance liquefiable soil layers interbedded with non-liquefiable layers, the presence of non-liquefiable crust above the critical layer, and the absence of thick clean sand layers are among the most typical characteristics of sites in Papanui and other western suburbs of Christchurch that did not show or showed only minor liquefaction manifestation at the ground surface during the 2010–2011 CES, contrary to the prediction of severe liquefaction by the simplified liquefaction evaluation procedures.

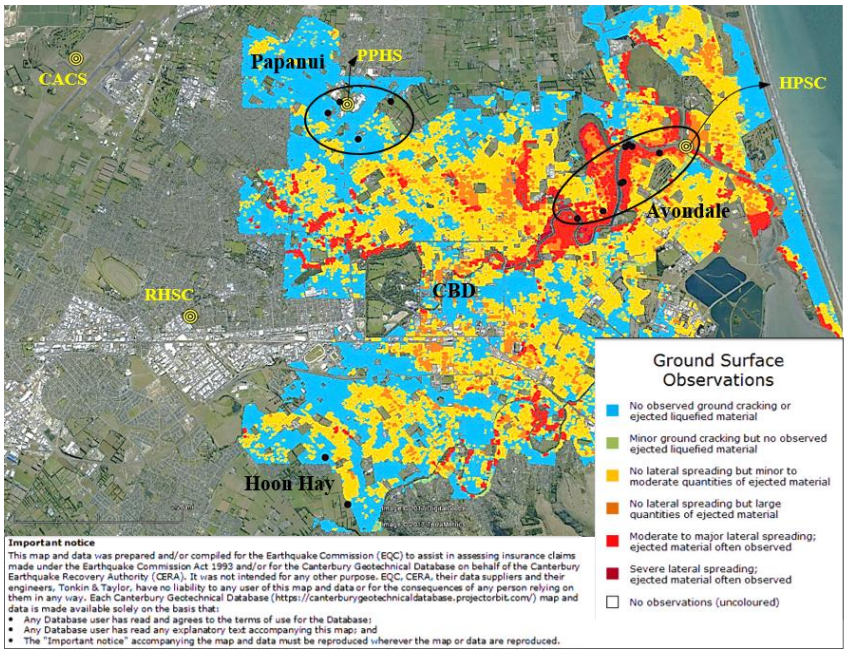


Figure 1. Liquefaction–induced land damage observations across Christchurch after the 22 February 2011 earthquake (NZGD, 2013), along with the locations of the selected sites (black symbols) and strong motion stations of interest (yellow spirals). The black ovals indicate the two considered sub-regions.

### *2.2 Avondale subsurface profile*

Sites in Avondale are primarily composed of alluvial sands and silts deposited by the Avon River which are underlain by near-shore marine and coastal sands and silts (Brown and Weeber, 1992). The top of the Riccarton Gravel is encountered at a depth of about 30–35 m from the ground surface and is often overlaid by a zone of soft soils with siltier composition ($I_c \approx 2.2$; McGann et al. 2017). Figure 2b shows the top 10 m of the subsurface soil profile of a typical Avondale site. The soil profile is characterized by vertically

continuous liquefiable soils, relatively highly permeable sand with no or low (non-plastic) fines content below 3.3 m, and absence of non-liquefiable plastic soil layers, including the absence of a non-liquefiable crust. A thick critical zone of clean sand to sandy silt ($I_c$ = 1.6–2.2) is located immediately below the shallow water table at about 1.5 m depth and extends up to 5.2 m. The vertical continuity of highly permeable liquefiable materials, the absence of non-liquefiable layers and the presence of a relatively low resistance and thick critical zone at shallow depths are key features encountered in the majority of the investigated sites in Avondale that manifested moderate-to-severe liquefaction in the September 2010 and February 2011 earthquakes and repeatedly liquefied in the two subsequent major events (i.e. June 2011 and December 2011 earthquakes).

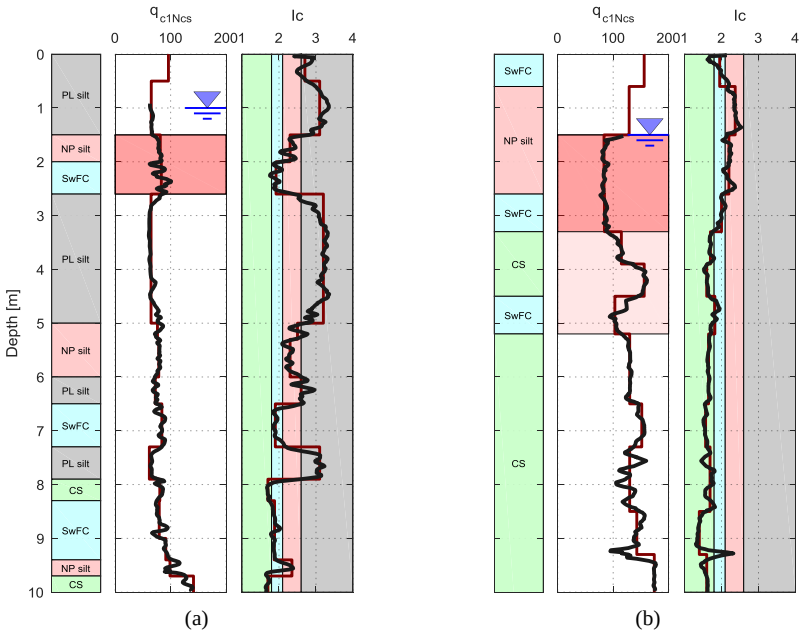


Figure 2. Typical $q_{c1Ncs}$ and $I_c$ profiles in (a) Papanui and (b) Avondale.

## 3. PROBABILISTIC MODELLING OF SOIL PROFILES

The employed probabilistic modelling of soil profiles is based on decoupling the layering generation (i.e. location and thicknesses of layers) from the definition of soil layer properties. The model builds upon Toro's (1995) idea for characterizing the random soil stratigraphy as a non-homogeneous Poisson process, whereas it utilizes nonparametric kernel distributions and a cross-correlation structure to determine the variation of soil properties within each layer.

### *3.1 Layering simulation*

Poisson processes are often used in engineering applications to model randomly occurring events over time or space. For a homogeneous Poisson process the mean rate of events is constant while for a non-homogeneous Poisson process the rate varies. For the layering problem under consideration, the event is a layer boundary (or layer interface) and its rate represents the number of layer boundaries per meter of length. Non-homogeneity was assumed to account for the fact that at certain site locations and depths (usually near-surface soils of the Springston formation) layers tend to be thinner (i.e. higher rate of layer boundary occurrence) than in the rest of the profile.

In this study, the rate function $\lambda(z)$ of the Poisson process (or alternatively, the cumulative rate function $\Lambda(z)$), where $z$ is the depth from the ground surface, is estimated from observations of layer boundary locations at selected sites of each sub-region using the nonparametric technique described in Arkin and Leemis (2000). Specifically, in this process six sites were used for the Papanui sub-region, whereas eight sites were used in Avondale. The selected site locations are indicated with the black symbols in the map of

Figure 1. Notice that two out of the six sites used for developing the probabilistic subsurface model of Papanui are located in Hoon Hay (southwest of the CBD). The shallow soil profile (< 10 m) in the Hoon Hay sites is very similar to that of Papanui; therefore, the inclusion of the two Hoon Hay sites does not create any complications, instead it increases the precision in the estimation of the rate function by increasing the number of observed realizations. That being said, it should be noted that in this preliminary study the focus was placed on designing the general probabilistic framework by scrutinizing few but well-characterized sites to understand the salient features of the subsurface profile in each sub-region and test the ability of the employed models to reproduce these features. To increase the reliability of the probabilistic analysis, additional sites as well as other Christchurch sub-regions will be included in future work.

For each of the selected sites, simplified soil profiles were determined using the available CPT data. The approach was to identify depth intervals over which the cone tip resistance ($q_c$) and the soil behavior type index ($I_c$) can be approximated by constant values, as illustrated with the solid red lines in the CPT profiles of Figure 2. On this basis soil layers and their corresponding thicknesses were defined while visual classification based on borehole data was also used as supporting information. The locations of layer boundaries identified as above for all sites within each sub-region were then used as overlapping realizations of the process (in superposition) for computing a piecewise-linear estimator of the cumulative rate function $\widehat{\Lambda}(z)$ (Arkin and Leemis, 2000). Once the cumulative rate function was defined, observations (i.e. locations of layer boundaries) for Monte Carlo simulation could be easily generated by transforming random event (layer boundary) locations from a unit Poisson process, $E_1$, $E_2$, … to the event (layer boundary) locations of the non-homogeneous Poisson process via the inverse cumulative rate function, $T_i = \Lambda^{-1}(E_i)$.

The procedure described above was used for generating layer boundaries in the upper 11 m of the deposit. These shallow parts of the deposit are the most important from a liquefaction manifestation viewpoint and therefore require detailed characterization and modelling. A slightly different approach was used for the layering simulation below 11 m. First, main boundaries were located by identifying depth intervals over which the soil behavior type index exhibits abrupt changes. To this end, the region–specific $I_c$ profiles developed by McGann et al. (2017) were used. The variation in the location of the main layer boundaries within the specified depth intervals was assumed to follow a uniform distribution. Once the main layer boundaries had been established, additional secondary layer boundaries were generated based on a homogeneous Poisson process with mean rate function $\lambda = 0.4$ (layer boundaries per meter). In addition, to avoid the generation of very thin soil layers which would require very fine mesh discretization in numerical modelling, a minimum layer thickness was defined at 0.30 m for the top 11 m and 0.50 m below.

Finally, the depth to Riccarton Gravel which constitutes the base layer in the numerical simulations, was assumed to follow a uniform distribution bounded by the minimum and maximum depths to Riccarton Gravel for the selected sites within each sub-region.

### *3.2 Definition of soil layer properties*

After the layering has been defined, the complete soil profile can be obtained by assigning the required soil properties to each layer. In effective stress analysis, liquefaction resistance curves (LRC) are typically used as the key parameter in the calibration of constitutive models for sandy soils. In the absence of site-specific laboratory tests, LRCs can be established from the CPT data using common empirical liquefaction triggering procedures (e.g. Boulanger and Idriss, 2014), as demonstrated by Cubrinovski et al. (2017). In this regard, the main two parameters required for characterizing the upper 11 m of potentially liquefiable soils are: the cone tip resistance, $q_c$ and the friction resistance, $f_s$.

It is apparent that $q_c$ and $f_s$ are correlated. For a given soil type higher values of the stress-normalized cone tip resistance $Q_{tn}$ are generally associated with higher values of the normalized friction ratio $F_r$ (positive correlation). On the other hand, a set of $Q_{tn}$–$F_r$ observations from varying soil types will most probably exhibit negative correlation. In Figure 3, $q_c$ and $I_c$ profiles from the considered sites in Papanui (Figure 3a) and Avondale (3b) are illustrated with the solid red lines. It can be seen from the $I_c$ traces that at a given depth the soil type may be identical or vary substantially among the considered sites. For example, in Avondale, from 4 to 9 m depth all soil profiles show clean sand type behavior index ($I_c \approx 1.5$–$2.0$) whereas at

shallower depths (above 3 m) the soil type behavior index varies from clean sand ($I_c \approx 1.8$) to silt or clayey silt ($I_c \approx 2.6$–$3.0$). In the former case, $Q_{tn}$–$F_r$ are positively correlated whereas in the latter case their correlation is negative. Therefore, the use of a single correlation coefficient cannot effectively describe the $Q_{tn}$–$F_r$ dependency at all depths. Similarly, the use of a unique theoretical probability distribution to describe the variation in $q_c$ and $f_s$ (or alternatively $Q_{tn}$ and $F_r$) does not seem appropriate. For instance, the commonly used normal distribution might work well in the Avondale sub-region, but would largely fail to model the variation of $q_c$ (or $I_c$) at depths about 4 m or 8–9 m in Papanui, where the observations are lumped around two discrete and distant (from one another) values.

Taking the above into consideration, a number of different probability distributions and correlation models, respectively, were investigated to describe the variation and dependency of $Q_{tn}$ and $F_r$. The dataset used for defining the probability distribution at each layer of a simulated profile was based on the $Q_{tn}$–$F_r$ data from the actual sites at the particular depth interval defined by the layer boundaries. Each model was assessed by examining whether the simulated soil profiles reflect the main features of the subsurface profile in the two sub-regions. The best representations of the soil profiles were obtained when both $Q_{tn}$ and $F_r$ were described by nonparametric kernel distributions. Rather than selecting a density with a particular parametric form and estimating the parameters, the kernel distribution produces a nonparametric probability density estimate that adapts itself to the data. Specifically, the kernel distribution builds the probability density function by creating an individual probability density curve for each data value and then summing up the smooth curves. This creates one smooth and continuous probability density function for the given data-set. Once the marginal kernel distributions for $Q_{tn}$ and $F_r$ had been specified, their correlation was provided with the use of copulas (e.g. Nelsen, 2006). A copula is a multivariate probability distribution, where each random variable has a uniform marginal distribution on the unit interval [0,1]. Bivariate Gaussian copulas were used in this study. In the bivariate Gaussian copula the dependence between the two random variables can be expressed by the use of rank correlation coefficients, such as the Kendall's $\tau$ correlation coefficient (Kendall, 1948). Kendall rank correlation coefficients $\tau$ of the normalized CPT variables ($Q_{tn}$ and $F_r$) were calculated separately for each layer of a simulated soil profile using the data from all sites within each sub-region. With the definition of the marginal distributions of $Q_{tn}$ and $F_r$ and their rank correlation at each layer of a simulated profile, dependent random $Q_{tn}$ and $F_r$ pairs were generated by first generating random numbers from the Gaussian copula, and then transforming these numbers into random $Q_{tn}$–$F_r$ values from the desired kernel distributions with the desired rank correlation using the inverse cumulative distribution functions of the kernel distributions for $Q_{tn}$ and $F_r$.

So far the discussion in this section has been focused on the definition of soil layer properties ($Q_{tn}$ and $F_r$) for the upper 11 m of the deposit. Soil layers below 11 m were modelled as non-liquefiable layers with their small-strain elastic behavior characterized by the shear wave velocity $V_s$ and their nonlinear behavior characterized by strain–dependent modulus degradation and damping ratio curves which, in turn, depend on the soil type (primarily the Plasticity Index, PI; Darendeli, 2001) and effective confining stress. At each layer, $V_s$- and $I_c$-values (the latter used as a proxy for defining the soil type and roughly estimating its PI) were randomly generated from the depth-dependent $V_s$ and $I_c$ distributions for Papanui and Avondale defined by McGann et al. (2017). The correlation between $V_s$ and $I_c$ was again taken into consideration through the use of Gaussian copulas as described above.

### *3.3 Simulated soil profiles*

Figure 3 shows with gray lines one hundred samples of randomized soil profiles in terms of $q_c$ and $I_c$ for Papanui (3a) and Avondale (3b). The corresponding profiles for the actual sites (red lines) are also shown for comparison.

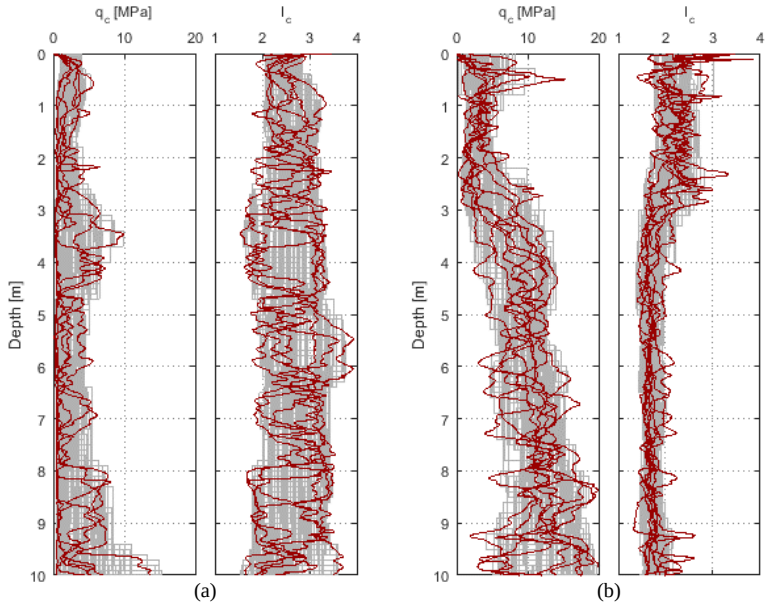


Figure 3. One hundred samples of randomized soil profiles (gray lines) for (a) Papanui and (b) Avondale. The red lines indicate the actual profiles used for the design and calibration of the probabilistic model in each sub-region.

As aforementioned, the methodology for the randomization of soil profiles was assessed by considering a random sample of the simulated soil profiles and examining whether this replicates the characteristics of the actual sites. To further assess the ability of the employed probabilistic soil profile modelling to reproduce the characteristics of the actual sites, simplified liquefaction analyses were performed and liquefaction damage indices, such as LPI, LSN, and $S_{v1D}$ (i.e. 1-D free-field post-liquefaction reconsolidation settlement) were comparatively examined. Figure 4 presents box and whisker plots depicting the range of variation in LPI, LSN, and $S_{v1D}$ for the actual sites (Figure 4a) in comparison with the corresponding ranges of variation for the generated soil profiles through simulations (Figure 4b). As can be seen, the median values (red lines) of the liquefaction damage indices are in excellent agreement between the actual and simulated profiles. Also, as expected considering the large number of simulated profiles in comparison with the actual ones, the former show a somewhat larger variation, which is certainly a desirable feature.

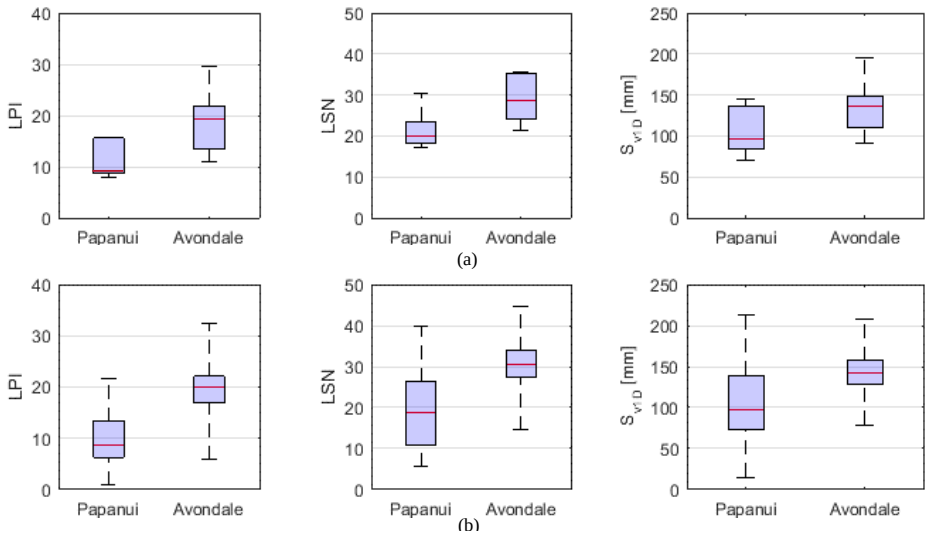


Figure 4. Comparison of the variation in liquefaction damage indices between (a) the actual soil profiles, and (b) the simulated soil profiles.

## 4. UNCERTAINTY IN GROUND MOTION

Typically in site response analyses the input motion at the base of a numerical model is obtained from recorded motions at nearby outrcropping rock site(s). In Christchurch, the absence of representative "rock" outcropping motions hinders such an approach. In past studies of the Canterbury earthquakes (e.g. Markham et al. 2016; Ntritsos and Cubrinovski, 2018), deconvolution of recorded surface motions (at soft soil sites) to the underlying stiffer Riccarton Gravel layer has been used to define the base input motions for 1D soil-column models. An alternative approach to deconvolution is to use "rock" motions at the desired locations obtained from physics-based ground motion simulations for the earthquake of interest (Razafindrakoto et al. 2016). Whatever the adopted approach is, one should expect a significant uncertainty associated with it.

In this study, both recorded and simulated motions are utilized. The Papanui High School (PPHS) and the Hulverstone Drive Pumping Station (HPSC) strong motion station (SMS) sites were chosen as reference sites for defining representative ground motions for Papanui and Avondale, respectively. The locations of these sites are illustrated with the yellow spirals in the map of Figure 1. There is no particular reason for selecting PPHS and HPSC as reference sites apart from the fact that simulated motions at these sites were readily available from another study, and that the SMS sites are within the two regions of interest. Details on the method used for extracting the simulated motions at the level of the Riccarton Gravel can be found in Razafindrakoto et al. (2016) and de la Torre et al. (2017). Base motions from the recorded accelerations at the ground surface were obtained via deconvolution analysis at two SMS sites: the Canterbury Aero Club (CACS) and the Riccarton High School (RHSC). The locations of these sites are also indicated in Figure 1. Both of these sites did not show any surface manifestation of liquefaction during any of the CES events and is believed to have shown only minimal nonlinear response during shaking (Markham et al. 2016); hence, they are suitable for deconvolution analysis using the equivalent linear approach. To account for differences in the site-to-source distance between the deconvolution sites (CACS and RHSC) and the sites of interest (PPHS and HPSC), the deconvoluted motions were scaled using a New Zealand–specific ground motion prediction equation as a basis (Bradley, 2013; Markham et al. 2016). A single scale factor was calculated as the ratio of the predicted (rock) spectral acceleration at the site of interest over the predicted (rock) spectral acceleration at the deconvolution site, averaged across a period range from 0.1 to 5.0 sec. Acceleration response spectra of the fault-normal component of the base motions, obtained as above, are shown for the two reference sites in Figure 5. The scale factors used in scaling the deconvoluted motions at CACS and RHSC are also annotated in this figure. Clearly, there are considerable differences between the three motions (CACS-based, RHSC-based and simulated), particularly at periods lower than 0.2 sec as well as in the period range between 1.5 and 3.0 sec. We have no reason to trust one motion more than another, therefore both record-based and simulated motions were used in the probabilistic analysis and were given equal probability of occurrence (0.5 for the simulated motion, 0.25 for the CACS-based motion, and 0.25 for the RHSC-based motion). In addition, to account for the uncertainty in the estimation of the scaling factor as well as the potential differences in the ground motion intensity between the reference sites and other sites in the considered sub-regions, the three base accelerations were multiplied by an additional normally distributed random scaling factor with mean $\mu = 1.0$ and standard deviation $\sigma = 0.20$.

Thus, the probability of occurrence of a specific ground motion and scaling factor can be computed by combining the above probability distributions. For example, a CACS-based motion with (additional) scaling factor between 0.8 and 1.20 has 0.68 x 0.25 = 0.17 = 17 % probability of occurrence. To prevent unrealistically high or unrealistically low accelerations a distribution truncation at $\pm 2\sigma$ was adopted for the additional scaling factor. Note that in this case, the exact value of the probability of occurrence in the given example will be somewhat different from the value reported above.

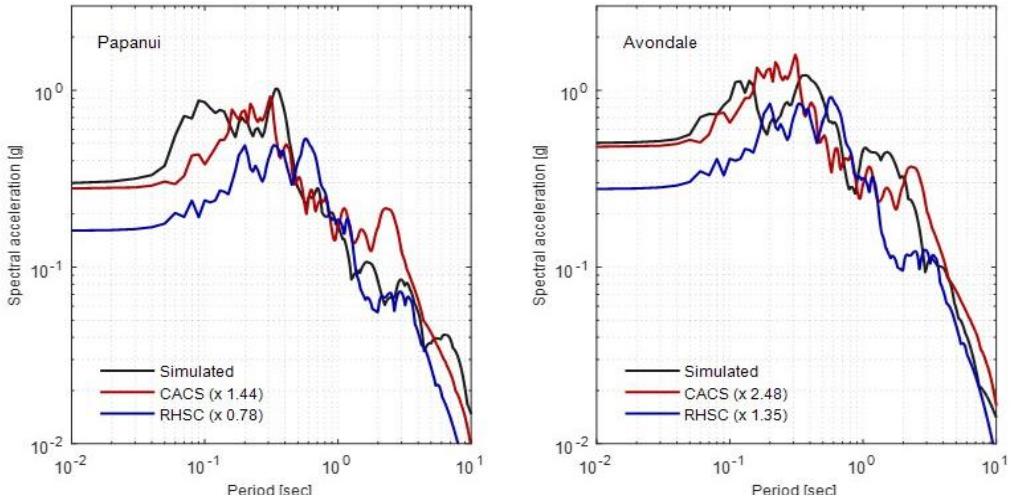


Figure 5. Acceleration response spectra of the base motions used in the probabilistic effective stress analyses.

## 5. ANALYSES AND RESULTS

### *5.1 Analysis methodology*

Each of the 100 generated random soil profiles in each sub-region was analyzed under 20 base input motions sampled from the combined ground motion distribution using a Latin Hypercube Sampling technique (McKay et al. 1979). In total, 2000 fully coupled effective stress (1-D soil column) analyses were performed for each sub-region. In the effective stress analyses, an advanced elastic–plastic constitutive model was used to simulate the liquefaction response of sandy soil layers (Cubrinovski and Ishihara, 1998a; 1998b). The so-called Stress–Density model (SD Model) is a state-concept based model that accounts for the combined effects of density and confining stress on sand behavior through the state-concept framework. The SD Model parameters were determined through a combined use of empirical relationships and generic data for sandy soils. More specifically, Christchurch sands were modelled using model parameters established from laboratory tests on Toyoura sand as a basis (Cubrinovski and Ishihara, 1998a; 1998b). The dilatancy parameters of the model were then slightly modified to simulate target LRCs established based on the liquefaction triggering procedure of Boulanger and Idriss (2014). The same set of SD parameters was used to simulate the target LRCs across all different density–stress states of liquefiable soil layers within the 200 simulated profiles, by only changing the initial void ratio as a function of $q_{c1Ncs}$. Non-liquefiable layers were also modelled with the SD Model except that the pore pressure generation feature was turned off for these layers. The shear stress–shear strain relationships were defined in these layers based on model simulations of the generic stiffness degradation and damping ratio curves proposed by Darendeli (2001). Further details on the adopted modelling approach can be found in Cubrinovski et al. (2017) and/or Ntritsos and Cubrinovski (2018).

In the following paragraphs selected results from deterministic effective stress analyses are first presented in order to briefly discuss the prevalent system response mechanisms for each soil profile typology. Then, the probabilistic analysis results are presented and interpreted in relation to the identified response mechanisms.

### *5.2 Deterministic analysis results*

Figure 6 shows excess pore water pressure isochrones for the two (deterministic) soil profiles described in Figure 2, caused by a CACS-based motion excitation with a scaling factor equal to 1.0.

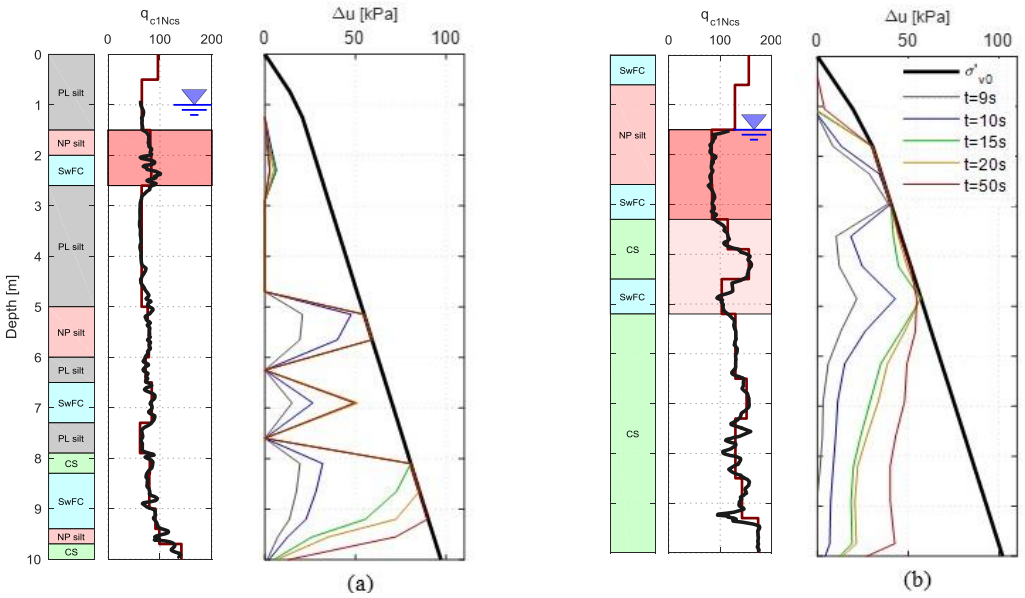


Figure 6. Evolution of excess pore water pressures for the (deterministic) soil profiles of Figure 2 under a CACS-based motion excitation: (a) Papanui site; (b) Avondale site.

The Papanui site (Figures 2a and 6a) has a critical layer from 1.5 to 2.6 m depth (from a liquefaction manifestation viewpoint), but note that all low resistance liquefiable layers are relevant for liquefaction triggering and its consequent effects on the dynamic response of the deposit. The effective stress analysis results show that significant excess pore water pressures develop within the non-plastic silt layer from 5 to 6 m depth at time $t$ = 10 s after only a few cycles of strong shaking, and full liquefaction has been triggered in this layer at $t$ = 15 s. It is not clear whether liquefaction would have occurred in the shallow critical layer if liquefaction at depth was prevented, but certainly the liquefaction of the non-plastic silt layer at 5–6 m depth reduced the seismic demand for all soils above these layers, as indicated by the drop in the excess pore water pressure of the shallow critical layer after $t$ = 15 s. This response is in accordance with the absence of surface liquefaction evidence in the site area.

The Avondale site (Figures 2b and 6b) has similarly a critical layer of low resistance ($q_{c1Ncs} \approx 84$) from 1.5 to 3.3 m. The shaking causes rapid development of excess pore water pressures all throughout the deposit and in this case liquefaction occurs first at $t$ = 10 s within the bottom part of the critical layer. The subsequent strong loading cycles from 10 to 15 s spread the liquefaction across a critical zone from 1.5 m immediately below the water table to about 5.2 m depth with the exception of the higher penetration resistance soils from 3.3 to 4.5 m. The latter, although having developed very high excess pore water pressures ($r_{u,t=15s} \approx 0.9$) at time $t$ = 15 s, they manifest complete liquefaction ($r_{u,} \approx 1.0$) only after 30 s with the contribution of water flowing from the early liquefied layer lying immediately underneath. The same effect of excess pore water pressure redistribution results in gradual increase of the excess pore water pressures in the top part of the deposit (above the initial water table depth of 1.5 m) due to water flow from the liquefied critical layer towards the ground surface. Relatively high excess pore water pressures are also developed at depths greater than 5.2 m and one can expect that under slightly higher seismic demand or slightly lower penetration resistance, these soils could also generate additional upward flow of water into the critical zone exacerbating the fluidization and instability of the soil structure within the latter (Cubrinovski et al. 2017). Moderate-to-severe liquefaction manifestation was observed at this site after the 22 February 2011 earthquake. This is in accordance with the predicted liquefaction of the thick and shallow critical zone and the progressive softening and potential seepage–induced liquefaction of the liquefiable soils above the groundwater table.
A more detailed discussion on results from deterministic effective stress analyses of Christchurch deposits can be found in Cubrinovski et al. (2017) and Ntritsos and Cubrinovski (2018).

### *5.3 Probabilistic analysis results*

The maximum excess pore water pressure ratio $r_{u,max}$ and the maximum shear strain $\gamma_{max}$ obtained from the

2000 simulations in each sub-region are displayed in Figure 7 (gray lines), along with the median, 25$^{th}$ percentile and 75$^{th}$ percentile curves (red lines). Also shown in this figure are the corresponding $r_{u,max}$ and $\gamma_{max}$ profiles resulted from the above deterministic analyses (blue lines).

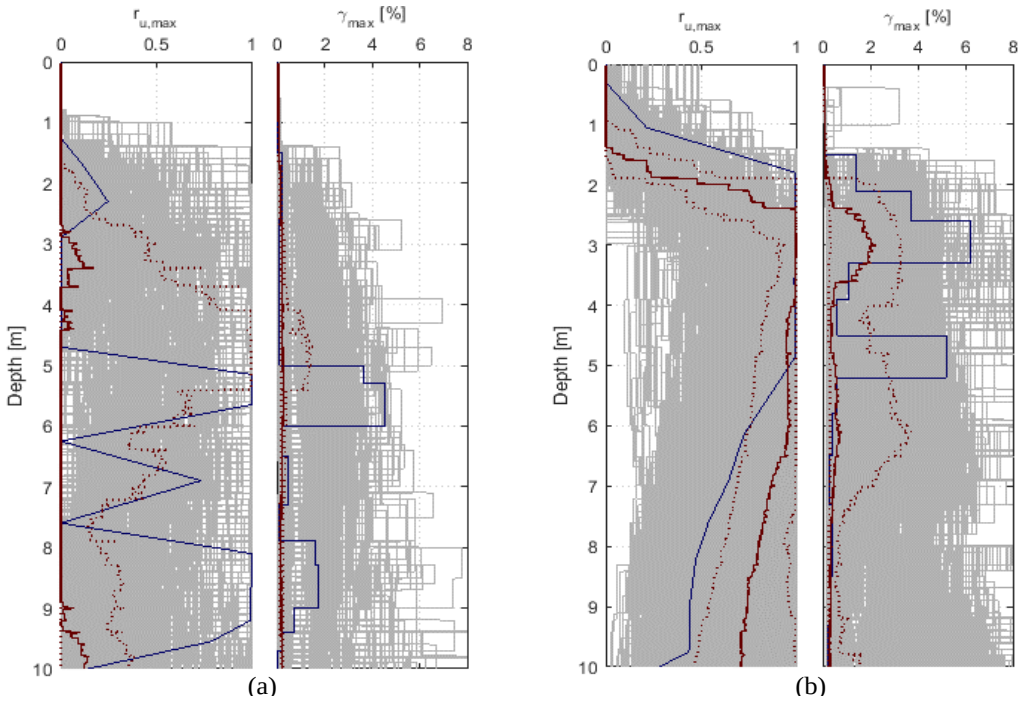


Figure 7. Variation in maximum excess pore pressure ratio $r_{u,max}$ and maximum shear strain $\gamma_{max}$ profiles for (a) Papanui and (b) Avondale. The solid red lines indicate the median response profiles whereas the dotted red lines indicate the 25$^{th}$ and 75$^{th}$ percentiles. The solid blue lines indicate the response profiles from the deterministic analysis (section 5.2).

In both cases, $r_{u,max}$ and $\gamma_{max}$ display a relatively large variability throughout the top 10 m of the soil deposit. By and large, the response in the Avondale sub-region is similar to that predicted by the deterministic analysis discussed in section 5.2. There exists a shallow and thick zone of liquefied soil ($r_{u,max} \approx 1.0$) at depth from about 2.2 m to 6.5 m overlying soils that did not completely liquefy but have developed high excess pore water pressures which also might be contributing to the severity of liquefaction with water inflow into the liquefied critical zone. On the other hand, the median response in the Papanui sub-region differs from that predicted by the deterministic analysis in that it implies that liquefaction does not occur at any depth in the deposit. However, a more thorough investigation of the effective stress analysis results reveals that nearly complete liquefaction ($r_{u,max} > 0.9$) has occurred at some depth in 85 % of the cases. The reason for this being concealed in the statistics of the response profiles presented in Figure 7a is that liquefaction does not always occur at the same depth but its depth of occurrence vary from profile to profile. Because the employed probabilistic modelling of soil profiles accounts for the variability in layer thicknesses and soil composition, the depth at which liquefaction is triggered in one or more of the simulated soil profiles may be corresponding to the presence of non-liquefiable layers in the remaining profiles; thereby shifting the $r_{u,max}$ and $\gamma_{max}$ statistical curves (median, 25$^{th}$ percentile, and 75$^{th}$ percentile) toward zero. That being said, it is here a good opportunity to emphasize the need for deterministic analyses to always be preceding probabilistic ones because the latter due to the abovementioned 'averaging of responses', very often, cannot exemplify mechanisms that might be crucial for the system response of deposits and can therefore mislead the interpretation of results.

To elucidate this aspect of the probabilistic analyses, an alternative illustration of the probabilistic analysis results is presented in Figure 8 where characteristics of the liquefaction response are depicted with box-and-whisker plots. In these plots, the depth indicates the depth to the top of the liquefied zone, the thickness is the thickness of the liquefied zone, and $\gamma_{max}$ is the maximum shear strain within the liquefied zone. The liquefied zone is defined as a continuous zone with $r_{u,max} > 0.9$. In cases where two or more liquefied zones (separated by non-liquefied layers) developed, the shallowest zone is only considered in the calculations. Data points

greater than $q_3 + 1.5\ (q_3 - q_1)$ or less than $q_1 - 1.5\ (q_3 - q_1)$, where $q_1$ and $q_3$ are the 25th and 75th percentiles of the data, are considered as outliers and are not included in the whiskers.

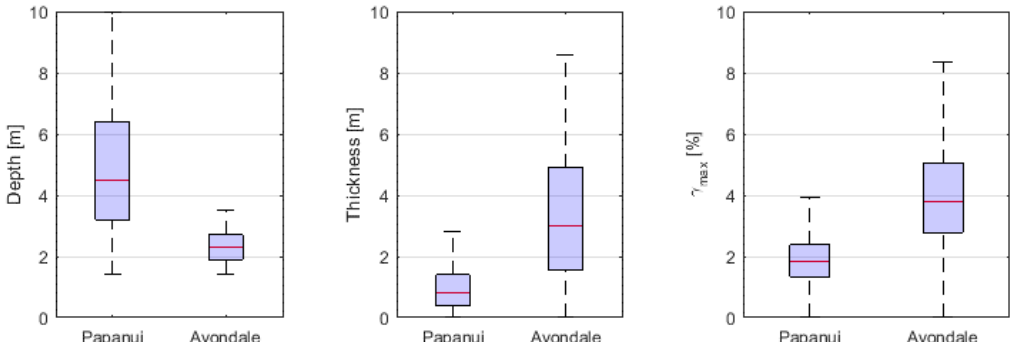


Figure 8. Variation in depth and thickness of the liquefied zone, and severity of liquefaction ($\gamma_{max}$).

In the above representation of the probabilistic analysis results the differences between the two sub-regions become evident. Location, extent (thickness) and severity of liquefaction play an important role in the severity of liquefaction manifestation at the ground surface. In Avondale, liquefaction occurs at shallow depth, about 2 to 3 m from the ground surface encompassing relatively thick zones (2–5 m) of severely ($\gamma_{max}$ ≈ 3–5 %) liquefied soils. In contrast, the average response of the Papanui sub-region is characterized by moderate liquefaction ($\gamma_{max}$ ≈ 2 %) of a thin layer (~ 1 m) overlaid by 3 to 6 m thick crust of non-liquefied soils. These results are in very good agreement with the actual observations from the 22 February 2011 earthquake (Figure 1), suggesting moderate-to-severe liquefaction manifestation in Avondale and absence of liquefaction or (occasionally) minor liquefaction manifestation in Papanui.

## 6. CONCLUSIONS

A probabilistic procedure for assessment of liquefaction–induced damage in urban areas was presented. The procedure uses Monte Carlo simulations and advanced effective stress analyses to estimate the statistics of the liquefaction response at a given (sub-)region due to variation in the soil profile and input ground motion. The general framework was illustrated through its application to assess the liquefaction performance of two sub-regions of Christchurch under the shaking induced by the 22 February 2011 Christchurch earthquake.
Selected results from deterministic effective stress analyses on representative sites from the two sub-regions were briefly discussed in order to highlight the importance of system–response mechanisms for the severity of liquefaction manifestation at the ground surface. In the Papanui sub-region, soil deposits are characterized by vertical discontinuity of the liquefiable layers, including low permeability non-liquefiable layers interchangeably sequencing relatively thin liquefiable layers. This type of soil profiles is affected by dynamic cross-interaction between layers, where liquefaction in a deeper layer substantially reduces the demand for all soils above that depth. As a result, sites in Papanui either did not manifest or manifested only minor liquefaction at the ground surface during the 22 February 2011 earthquake despite the presence of multiple liquefiable layers of low resistance. In the Avondale sub-region, soil deposits are characterized by vertically continuous liquefiable materials throughout the depth of the profile. In this type of soil profiles, liquefaction first occurs at shallow soils of low penetration resistance. Soon after, the water flow from the liquefied layers towards the ground surface and from deeper soils of higher resistance into the liquefied zone causes either seepage–induced softening and potential liquefaction of otherwise stable soils or additional disturbance of already liquefied layers. Such deposits manifested moderate-to-severe liquefaction during the 22 February 2011 earthquake and repeatedly liquefied in all major events of the 2010–2011 Canterbury earthquake sequence.

The probabilistic analysis results show a relatively large range of variation in the liquefaction response, yet the response of the two sub-regions is clearly distinct. It was shown that the representation of the probabilistic analysis results only in terms of median response profiles can often lead to wrong conclusions. Therefore extra care must be taken in the interpretation of results from probabilistic analysis, and the latter

should always be preceded by detailed deterministic analyses. The two sub-regions show substantial differences with respect to the location, extent and severity of liquefaction within the deposit. In Avondale, liquefaction occurs at shallow depth and encompasses thick zones of severely liquefied soil. In Papanui, liquefaction occurs at thin layers located at larger depths and overlaid by thick crusts of non-liquefied soils. Clearly, the location, extent and severity of liquefaction play an important role in the severity of liquefaction manifestation at the ground surface.

By and large, the outcomes of the probabilistic analysis are in very good agreement with the actual observations of liquefaction–related damage from the 22 February 2011 earthquake. As more sites and more sub-regions are added in the probabilistic models of soil profiles, the reliability of the probabilistic analysis results will be increasing. This will allow for the proposed probabilistic framework to be used with confidence in assessing and mapping the expected liquefaction–induced damage in future earthquakes.

## 7. ACKNOWLEDGMENTS

The first author would like to acknowledge the EQC–QuakeCoRE scholarship. This study is part of the "55 sites" project funded by the Earthquake Commission New Zealand (EQC). The authors are also immensely grateful to Aimee Rhodes from Opus International Consultants Ltd, Sjoerd van Ballegooy from Tonkin+Taylor, Sarah Bastin, Chris McGann, Chris de la Torre, Hoby Razafindrakoto, Robin Lee and Brendon Bradley from University of Canterbury for their contributions to this study.

## 8. REFERENCES

Arkin BL, Leemis LM (2000). Nonparametric estimation of the cumulative intensity function for a nonhomogeneous Poisson process from overlapping realizations. *Management Science, 46*(7), 989-998.

Boulanger RW, Idriss IM (2014). CPT and SPT based liquefaction triggering procedures. Report No. UCD/CGM-14/01, Centre for Geotechnical Modeling, Department of Civil and Environmental Engineering University of California, Davis.

Bradley BA (2013). A New Zealand-specific pseudospectral acceleration ground-motion prediction equation for active shallow crustal earthquakes based on foreign models. *Bulletin of the Seismological Society of America, 103*(3), 1801-1822. doi: 10.1785/0120120021

Brown L, Weeber J (1992). Geology of the Christchurch Urban Area. Scale 1:25 000. Institute of Geological and Nuclear Sciences geological map 1. 1 sheet + 105 p, Lower Hutt, New Zealand.

Cubrinovski M, Ishihara K (1998a). Modelling of sand behaviour based on state concept. *Soils and Foundations, 38*(3), 115-127.

Cubrinovski M, Ishihara K (1998b). State concept and modified elastoplasticity for sand modelling. *Soils and Foundations, 38*(4), 213-225.

Cubrinovski M, Robinson K (2016). Lateral spreading: evidence and interpretation from the 2010–2011 Christchurch earthquakes. *Soil Dynamics and Earthquake Engineering, 91*, 187-201. doi: 10.1016/j.soildyn.2016.09.045.

Cubrinovski M, Rhodes A, Ntritsos N, van Ballegooy S (2017). System response of liquefiable deposits. Paper presented at the PBDIII Earthquake *Geotechnical Engineering*, Vancouver, Canada.

Darendeli MB (2001). Development of a new family of normalized modulus reduction curves and material damping curves. *PhD Thesis*, University of Texas, Austin.

de la Torre CA, Bradley BA, Jeong S, McGann CR (2017). Incorporating soil nonlinearity into physics-based ground motion simulation through site-specific ground response analysis. P*aper presented at the PBDIII Earthquake Geotechnical Engineering*, Vancouver, Canada.

Idriss IM, Boulanger RW (2008). Soil liquefaction during earthquakes. Monograph MNO-12. Oakland, California: Earthquake Engineering Research Institute; 261.

Kendall MG (1948). Rank correlation methods. 4th Edition, Griffin, London, 1948.

Markham CS, Bray JD, Macedo J, Luque R (2016). Evaluating nonlinear effective stress site response analyses using

records from the Canterbury earthquake sequence. *Soil Dynamics and Earthquake Engineering, 82*, 84-98. doi: 10.1016/j.soildyn.2015.12.007

McGann CR, Bradley BA, Cubrinovski M (2017). Development of a regional $V_{s30}$ model and typical $V_s$ profiles for Christchurch, New Zealand from CPT data and region-specific CPT-$V_s$ correlation. *Soil Dynamics and Earthquake Engineering, 95*, 48-60. doi: 10.1016/j.soildyn.2017.01.032

McKay MD, Beckman RJ, Conover WJ (1979). Comparison of three methods for selecting values of input variables in the analysis of output from a computer code. *Technometrics, 21*(2), 239-245. doi: 10.1080/00401706.1979.10489755

Nelsen RB (2006). *An introduction to Copulas*. 2nd Edition, Springer, New York.

New Zealand Geotechnical Database (2013). Liquefaction and Lateral spreading Observations. Map Layer GCD0300 - 11 Feb 2013, retrieved 27 Nov 2017 from https://www.nzgd.org.nz/

Ntritsos N, Cubrinovski M (2018). *Evaluation of liquefaction case histories from the 2010-2011 Canterbury earthquakes using advanced effective stress analysis*. Paper submitted for presentation at the 5th GEESD Conf., Austin, Texas.

Razafindrakoto HNT, Bradley BA, Graves RW (2016). *Broadband ground motion simulation of the 2010-2011 Canterbury earthquake sequence.* Paper presented at the 2016 NZSEE Conf., Wellington, New Zealand.

Robertson PK, Wride CK (1998). Evaluating cyclic liquefaction potential using the cone penetration test. *Canadian Geotechnical Journal, 35*(3), 442-459.

Toro GR (1995). Probabilistic models of site velocity profiles for generic and site-specific ground-motion amplification studies. *Department of Nuclear Energy Brookhaven National Laboratory*, Upton, New York.

Youd TL, Idriss IM, Andrus RD, Arango I, Castro G, Christian JT, Stokoe KH (2001). Liquefaction resistance of soils: Summary report from the 1996 NCEER and 1998 NCEER/NSF workshops on evaluation of liquefaction resistance of soils. *Journal of Geotechnical and Geoenvironmental Engineering, 127*(20), 817-833. doi: 10.1061/(ASCE)1090-0241(2001)127:10(817)